	Coordinate MNI space				Cluster
Region	x	y	z	Z score	size
Left parahippocampal gyrus	−26	−42	−9	4.93	2391*
Left hippocampus	−28	−15	−14	4.22	

*Uncorrected $p<0.001$,
cluster level $p<0.05$ (corrected for multiple comparisons).

Fig. 3. Result of VBM analysis: In the left hippocampus and parahippocampal gyrus, only a significant cluster of gray matter density reduction in subjects with amnestic MCI who converted to AD within three years (MCI-C) compared to subjects who did not (MCI-NC) ($p<0.001$, uncorrected for multiple comparisons and $p<0.05$, cluster-level corrected for multiple comparisons).

while the accuracies shown in Fig. 7 were calculated with the 80 LOOCV results of different classifiers that were trained with different combinations of 37 features. These combinations of 37 features were similar but not identical to one another and to the fixed set based on the feature ranking. There were significant main effects and interactions of atlas and feature selection ($p<0.0001$) except between AAL and BA without feature selection ($p=0.16$).
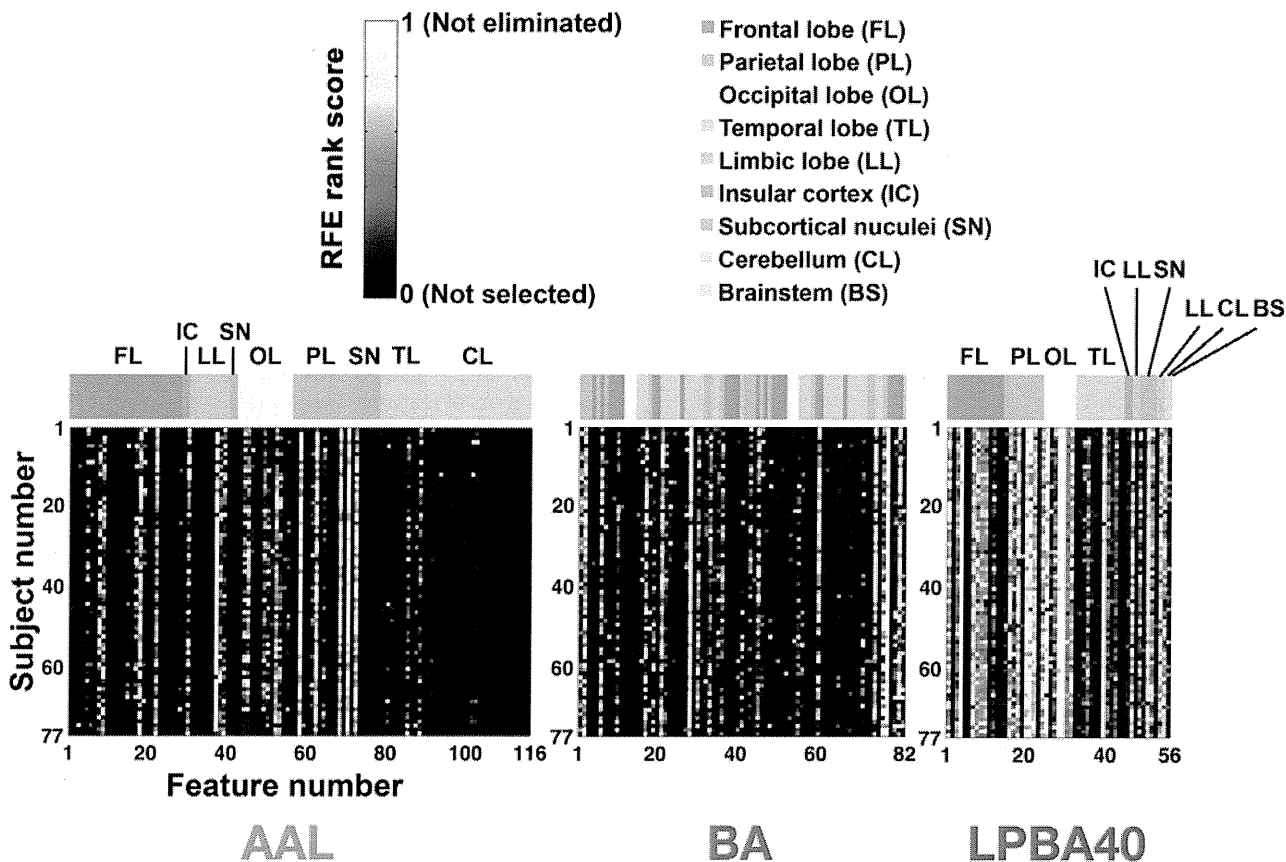
Fig. 4. RFE rank score matrices from three brain atlases. The vertical axis of the map represents the subject number, i.e., each step of the leave-one-out cross-validation (LOOCV) procedure. The horizontal axis represents the number of features in each atlas. The top-ranked features having a score of 1, i.e., the feature last selected during the SVM-RFE procedure, are colored in white, while the features that were not selected (score 0) are colored in black. AAL, Automated Anatomical Labeling; BA, Brodmann's areas; LPBA40, LONI Probabilistic Brain Atlas.
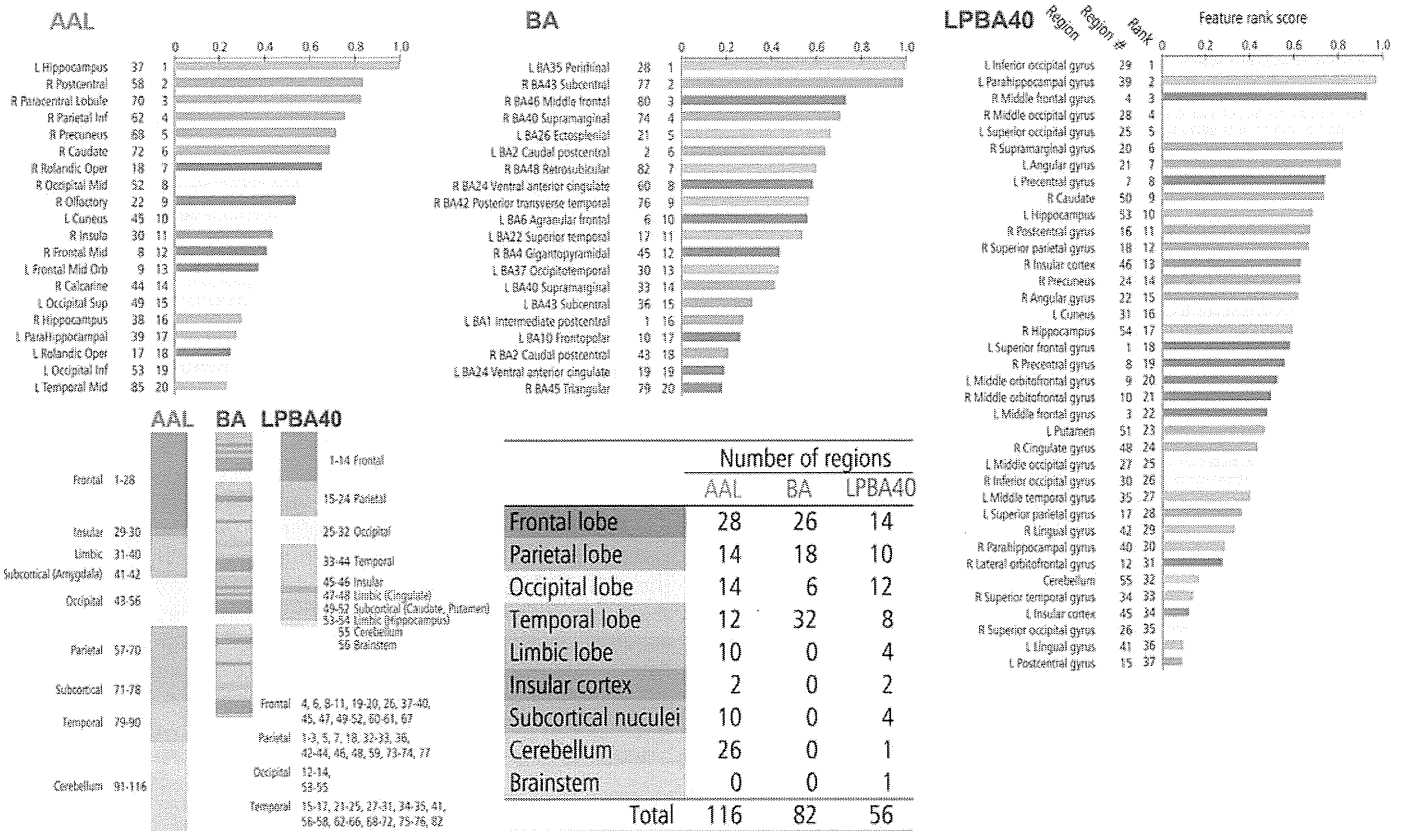
Fig. 5. Final rankings of features of three brain atlases and bar plots of feature rank score as a result of the SVM-RFE procedure. Each bar plot for each region is colored differently according to its anatomical location. AAL, Automated Anatomical Labeling; BA, Brodmann's areas; LPBA40, LONI Probabilistic Brain Atlas.

Fig. 9 shows ROC curves with AUC and 95% CI obtained with different atlases using the original features and the features further selected through the SVM-RFE procedure. All p-values for feature selection differences were smaller than 0.0001 in all the atlases. Without feature selection, p-values for atlas differences were 0.84 for AAL vs. BA, 0.0055 for AAL vs. LPBA40, and 0.014 for BA vs. LPBA40. In contrast, using feature selection, there were no significant differences ($p > 0.05$) between the pairs of atlases.

4. Discussion

This study focused on feature extraction using atlas-based parcellation and feature selection based on the SVM-RFE algorithm in SVM-based classification using GM volumes from baseline structural MRI of subjects with amnestic MCI. To date, we are not aware of any study that has demonstrated a comparison of brain atlases for feature extraction.
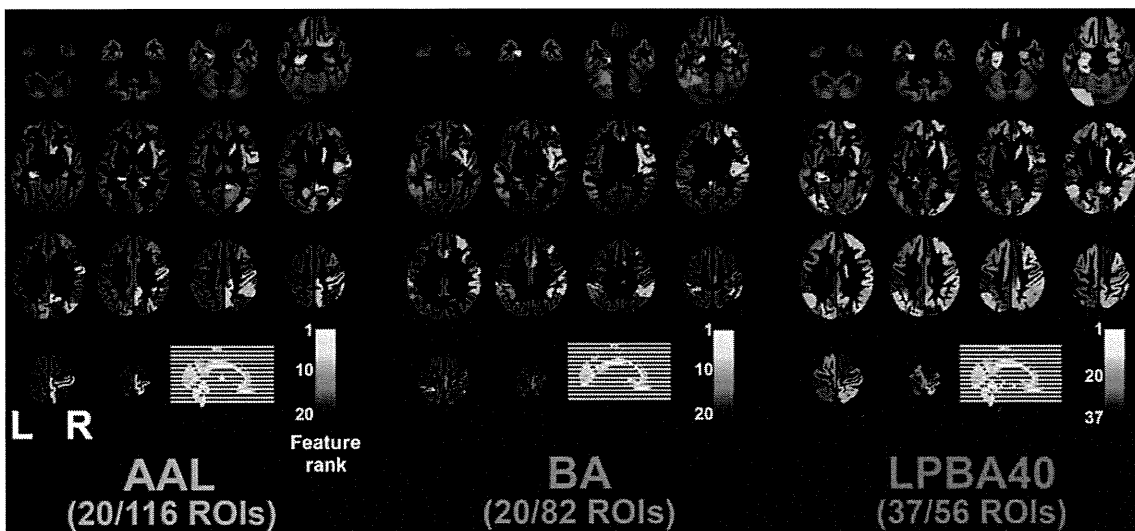

Fig. 6. Selected region maps from the SVM-RFE procedure, which revealed the highest performance, overlaid to representative structural MR images. The regions with the highest rank are colored in white and those with the lowest rank are colored in black. AAL, Automated Anatomical Labeling; BA, Brodmann's areas; LPBA40, LONI Probabilistic Brain Atlas.

Table 2

Results of SVM classification using the feature sets extracted with three brain atlases without feature selection and those with a feature selection method based on SVM-RFE. The feature selection technique enhanced the performance of the classification for all of the atlases.

Atlas	Without feature selection				With SVM-RFE			
	Number of features	ACC	SEN	SPC	Number of features	ACC	SEN	SPC
AAL	116	55.8%	56.4%	55.3%	20	71.4%	69.2%	73.7%
BA	82	54.5%	53.8%	55.3%	20	67.5%	64.1%	71.1%
LPBA40	56	67.5%	71.8%	63.2%	37	77.9%	76.9%	78.9%

SVM-RFE, support vector machine-based recursive feature elimination; ACC, accuracy; SEN, sensitivity; SPC, specificity; AAL, Automated Anatomical Labeling; BA, Brodmann's Areas; LPBA40, LONI Probabilistic Brain Atlas.
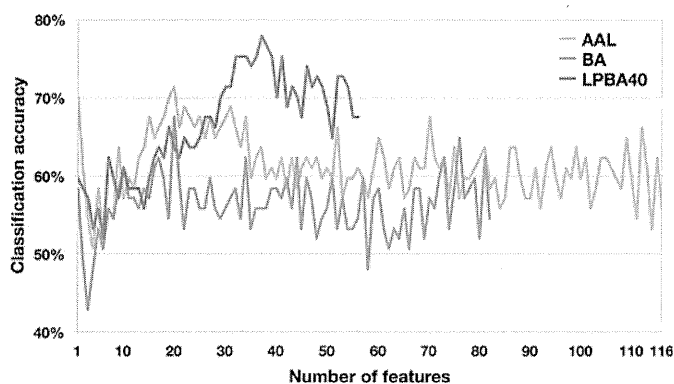

Fig. 7. Plots of the classification accuracy versus the number of features in the dataset extracted with each brain atlas. AAL, Automated Anatomical Labeling; BA, Brodmann's areas; LPBA40, LONI Probabilistic Brain Atlas.

The SEAD-J study showed a higher conversion rate for year 1 compared with the ADNI study (Kawashima et al., 2012). The inclusion criteria of SEAD-J were different from that of ADNI, for example, in WMS-R LM II score. The cohort of SEAD-J included amnestic MCI patients with severer verbal memory deficits compared with ADNI. Tabert et al. (2006) reported that deficits in verbal memory strongly predicted conversion to AD. Thus, this higher conversion rate might be due to the severity of memory deficit of the SEAD-J cohort, which is likely to be attributed to the inclusion criteria of SEAD-J.

We classified 77 subjects in this study into late MCI (LMCI) and early MCI (EMCI) on the basis of their objective memory loss measured by education-adjusted scores on WMS-R LM II according to the definition of LMCI and EMCI in the inclusion criteria of the ADNI 2 study (page 27 of the ADNI 2 Procedures Manual, http://adni.loni.ucla.edu/wp-content/uploads/2008/07/adni2-procedures-manual.pdf). As a result, 60 subjects (77.9% of total)

were classified into LMCI and 17 subjects (22.1%) EMCI. More specifically, 39 converters (MCI-C) in our study consisted of 37 LMCI (94.9%) and 2 EMCI (5.1%), whereas 38 non-converters (MCI-NC) included 23 LMCI (60.5%) and 15 EMCI (39.5%). The proportions of LMCI and EMCI between the MCI-C and MCI-NC groups were significantly different (Fisher's exact test, p-value = 0.00028).

The result of the VBM analysis was consistent with that of a previous meta-analysis of VBM studies (Ferreira et al., 2011). The correspondence could demonstrate the validity of the MRI data and the methodology of VBM that we used in this study. The results have their own limitations, which are derived from the MRI data being acquired on multiple scanners at different research institutions. After adjusting for interscanner variability in the quality of the MRI
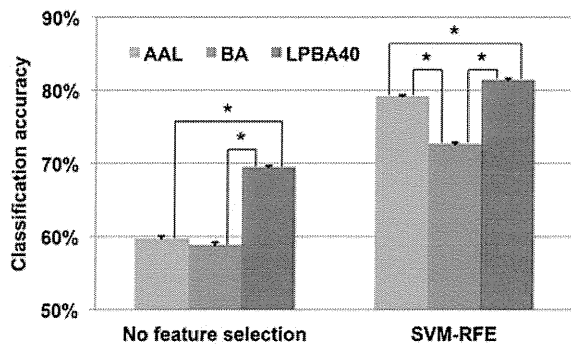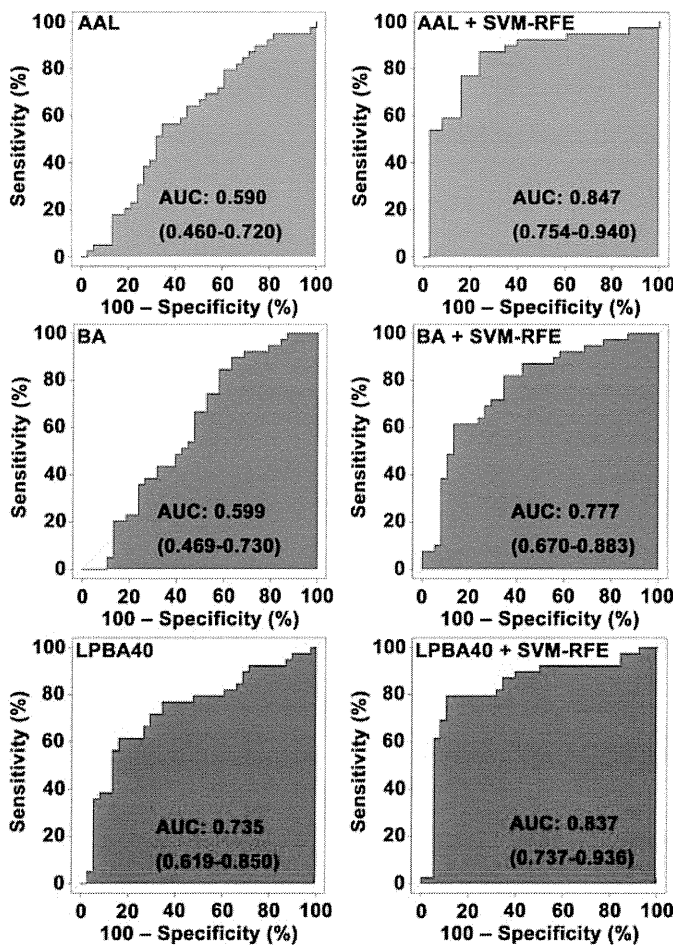

Fig. 8. Classification accuracies obtained with features extracted using different atlases (left) and features further selected through the SVM-RFE procedure (right). Values are mean and error bars represent standard errors. *$p < 0.0001$, two-way ANOVA followed by Tukey's multiple comparison test. AAL, Automated Anatomical Labeling; BA, Brodmann's areas; LPBA40, LONI Probabilistic Brain Atlas; SVM-RFE, Support vector machine-recursive feature elimination.

Fig. 9. Receiver operating characteristics (ROC) curves with the areas under the curve (AUC) and 95% confidence intervals (CI) obtained with different atlases using the original features and the features further selected through the SVM-RFE procedure. CIs for AUCs were computed with DeLong's method. SVM-RFE, Support vector machine-recursive feature elimination; AAL, Automated Anatomical Labeling; BA, Brodmann's areas; LPBA40, LONI Probabilistic Brain Atlas.

acquisitions in both VBM and SVM analyses, we obtained classification accuracies in the range of 55–78% (mean ± SD = 65.8 ± 9.1%) that were comparable with those of previous studies (56–82%, mean ± SD = 66.8 ± 7.0%) (Eskildsen et al., 2013). These results indicate that the effect of scanner differences on the results of this study might not be significant, as shown in a previous VBM study using MRI data from different scanners (Stonnington et al., 2008). In addition, because the goal of this study was to evaluate the relative differences in the classification performances of the different brain atlases, the MRI data from multiple scanners probably made no remarkable difference in the results of the comparison among the atlases.

We applied an LOOCV technique where a test set and a training set were initially separated before the SVM-RFE procedure. The training set at each step of the SVM-RFE did not include the test set. The cross-validation procedure may prevent the overfitting problem (Hsu et al., 2003). Thus, it may be unlikely that the classification accuracies we obtained are inflated accuracies due to overfitting.

Different atlases for parcellation may cause differences in feature vectors constructed from the original whole-brain volumetric image on the basis of the following major factors: (1) a method to parcel the whole brain and (2) number or size of regions. Different atlases having different number of ROIs provide different feature vectors having different inter-regional correlations (Wang et al., 2009; Faria et al., 2012). Multivariate analysis utilizes the spatial covariance structure in the data (Habeck et al., 2008). Differences in topological patterns of feature vectors in feature space thus may affect the decision boundary of a multivariate classifier. Accordingly, different inter-regional correlations due to different parcellation atlases can influence the classification accuracy in the multivariate pattern analysis.

The overall classification performance in this study was better than or comparable with the results of previous studies on the early prediction of AD using MRI-based biomarkers (Cuingnet et al., 2011; Davatzikos et al., 2011; Wolz et al., 2011; Cho et al., 2012; Eskildsen et al., 2013). The study demonstrated the classification performance differed across atlases when no feature selection was applied, using the same dataset and the same methods except for different atlases to define ROIs in voxel-based analysis. Although there were no significant differences in AUC, classification accuracies revealed significant differences across atlases when SVM-RFE was applied. To find the "optimal" atlas for AD prediction, however, replication in another cohort would be required to demonstrate that the found prediction accuracy was not merely by chance on the particular cohort studied.

Then, what are the reasons for providing such a considerable disparity in the performance across the three atlases? Although underlying causality remains unknown, clues for solving this question, if any, could be found in the differences between the atlases. The AAL and BA atlases with the "ch2" image gave similar classification accuracies, whereas LPBA40 with the ICBM452W5 template differed in their classification performance from the other two. Therefore, we mainly contrast AAL with LPBA40 for simplicity.

Brain atlases are classified into two categories: single-subject topological atlases and population-based probabilistic atlases (Cabezas et al., 2011). AAL is a single-subject atlas that is based on the brain of a young male (Tzourio-Mazoyer et al., 2002), whereas LPBA40 is a probabilistic atlas created from 40 MRI volumes (Shattuck et al., 2008). We speculate that this difference might be a major important difference between AAL and LPBA40. No single brain is representative of a population because of the neuroanatomical variability across individuals (Devlin and Poldrack, 2007). There is, therefore, no "correct" single-subject atlas. For example, the MNI single-subject brain has some problems because of anatomical variation and methodological limitations in spatial normalization.

Regarding anatomical variation, Tzourio-Mazoyer et al. (2002) mentioned that the MNI single-subject brain of AAL showed an atypical rightward asymmetry of the planum temporale (PT). The PT is a triangular structure that is located on the superior temporal gyrus (STG) and that has extensive connections to (and from) other regions of the brain. The PT could be engaged in mediating sensorimotor control processing such as speech motor processing (Zheng, 2009). PT asymmetry might be influenced by gender, and this rightward anatomical variation in the MNI brain of a young man was found in only approximately 10% of the subjects in a previous study (Shapleske et al., 1999). Chance et al. (2011) reported that microanatomical changes in cortical minicolumn organization of the association cortex in the PT (BA22) were detected in the early stages of MCI as well as AD. Such minicolumn measures in the temporal lobe reportedly reflect selective regional vulnerability to AD tangle pathology and differential involvement in the cognitive deficit of AD (Chance et al., 2006). Involvement of the superior temporal cortex in early atrophic changes in AD was also found in a VBM study on patterns of GM loss in MCI and AD (Karas et al., 2004). Furthermore, the SVM analyses in this study demonstrated that BA22 and STG in the right hemisphere were selected via the SVM-RFE procedure in BA and LPBA40, respectively, whereas in AAL, the STG in each hemisphere was eliminated. STG was also chosen by a feature selection method that was different from the SVM-RFE procedure for the classification of MCI using a linear discriminant analysis (Eskildsen et al., 2013). These findings suggest that the atypical PT asymmetry in the MNI single-subject brain might pertain to the relatively poor performance of a whole-GM SVM classification of MCI using AAL-based parcellation.

Tzourio-Mazoyer et al. (2002) also reported that several sulcal patterns in the MNI single-subject brain, such as the Rolandic sulcus and the precentral sulcus in the left hemisphere, had a low probability with reference to Ono's atlas of sulci (Ono et al., 1990). In AAL, the ROIs in each hemisphere were defined using sulcal landmarks as the limits of the ROIs on the outer surf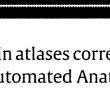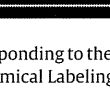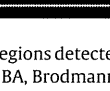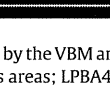ace of the brain. The internal limit of the regions was extended beyond the gray matter layer, because AAL was originally intended to provide a standard reference frame of anatomical localization for functional neuroimaging studies with generally lower spatial resolution compared to anatomical MRI (Tzourio-Mazoyer et al., 2002). However, sulcal and gyral patterns are extremely variable, and macroanatomical landmarks do not match cytoarchitectonic borders in almost all of the cases (Amunts et al., 2007). In fact, AAL provides peak labeling, not precise anatomical localization, for structural imaging studies (Tzourio-Mazoyer et al., 2007). Thus, a single-subject atlas such as AAL does not represent the individual diversity of human anatomy (Toga and Thompson, 2007; Cabezas et al., 2011).

These issues in AAL suggest that care must be taken to apply AAL to structural MRI analyses of subjects with MCI, as many experts suggested (Devlin and Poldrack, 2007; Toga et al., 2006; Toga and Thompson, 2007; Tzourio-Mazoyer et al., 2002, 2007; Evans et al., 2012).

Although LPBA40 better represents the MCI cohort in this study compared with AAL, LPBA40 might not be the best choice. Population-based templates also lack inter-subject correspondence in cortical folding (Mangin et al., 2010). Furthermore, LPBA40 also differed from the MCI cohort in this study in terms of age, race, and disease, which is similar to in AAL. Cortical thickness analysis with the surface-based atlases in FreeSurfer (Desikan et al., 2006; Destrieux et al., 2010; http://surfer.nmr.mgh.harvard.edu/) using the same dataset as in this study might provide improved classification performance. Future studies that use a disease-specific population-based atlas for MCI would also better serve the early detection of AD (Toga et al., 2006; Toga and Thompson, 2007).

Another difference between the atlases is the number of ROIs in each atlas. Although a left hippocampal region was detected

Atlas	Region	Feature #	Feature Rank	Region map
AAL	L PHG	39	17	
	L HC	37	1	
BA	L BA37	30	13	
	L BA20	15	46	
LPBA40	L PHG	39	2	
	L HC	53	10	

Fig. 10. Left parahippocampal regions and left hippocampal regions in three brain atlases corresponding to the regions detected by the VBM analysis. The left parahippocampal and the hippocampal regions are colored in white and red, respectively. AAL, Automated Anatomical Labeling; BA, Brodmann's areas; LPBA40, LONI Probabilistic Brain Atlas; L PHG, Left parahippocampal gyrus; L HC, Left hippocampus.

as a robust discriminating region by a univariate analysis (Fig. 3), our multivariate analysis demonstrated that classification using multiple features rather than a sole well-discriminating predictor could lead to better performance. When using the AAL atlas, the left hippocampus (Region 37) was most often selected as the last remaining feature after SVM-RFE. Using only this feature can provide a relatively good accuracy around 70% for the dataset we used in this study. In some circumstances, when adding more features, the resulting set of features may be more discriminating as a whole than the only feature in multivariate analysis. In other cases, the resulting set of features may be less discriminating than the original set and the resulting accuracy may be worse than when not adding the features. A set of features generated from 116 regions of the AAL atlas may generally contain a lot of less discriminating features. Therefore feature selection can be crucial when using atlases. A previous multivariate analysis of MR images of subjects with MCI also achieved improved accuracy in classification using linear discriminant analysis (LDA) with multiple features (Wolz et al., 2011). Our study suggests that an optimal number of regions could result in good performance in multivariate analysis and that too many regions also could lead to poor performance due to overfitting. However, it is difficult to determine the optimal number of regions in advance of feature extraction. During the SVM-RFE procedure, regions that do not contribute well to the separation are removed from the original feature set according to a feature-ranking algorithm. Whether an individual region separates the classes well or not is determined by how to parcellate a brain template. Multimodal probabilistic atlases generated by integrating the cytoarchitectonic, receptor architectonic and functional imaging data (Toga et al., 2006) will play an important role in MRI data analyses.

BA and AAL gave similar results in both the classification performance and the regions selected through the SVM-RFE procedure. A parcellation that is too coarse would not reflect the underlying cytoarchitecture in each coarse region, as Amunts et al. (2007) concluded from their classification results using unsupervised cluster analysis on seven occipital areas of ten human brains. One of the possible explanations for why BA has poorer performance compared with AAL was the coarse parcellation in BA, although

the ROI generation of BA by subdivision at the mid-sagittal plane might be imprecise. However, the poor classification performance in BA could primarily be attributed to the same problems in the MNI single-subject brain as in AAL, because LPBA40, which has the smallest number of regions, provided the best performance.

As seen from Figs. 5 and 6, the left hippocampal region was not consistently selected among the atlases. Fig. 10 shows the left parahippocampal region and left hippocampal region in each atlas corresponding to the regions detected by the VBM analysis shown in Fig. 3. The left hippocampal region differed across the atlases as shown in Fig. 10. Moreover, because the number of ROIs was also different among the atlases, correlations between the left hippocampal region and the other regions, i.e., correlation or covariance patterns also differed across the atlases. Multivariate analysis utilizes the spatial covariance structure in the data (Habeck et al., 2008). Different covariance patterns due to different atlas-based parcellations might cause the inconsistency in the selection of the left hippocampal region among the atlases as well as the differences in the performance of multivariate classifiers.

Similarly to this study, Chu et al. (2012) also employed similar methods for MCI prediction. Namely, they also used the LPBA40 atlas for atlas-based parcellation, the SVM-RFE method for feature selection, and SVMs for classification among AD, MCI, and normal controls. However, differently from our study, they basically adopted a voxel-wise data-driven feature selection approach using high-dimensional whole brain voxel data (299,477 voxels) as the original input features. Moreover, they used seven atlas-based ROIs and two combinations thereof as prior knowledge for feature selection. The regions were chosen arbitrarily based on findings from previous mass-univariate VBM analyses. The classification accuracies using different ROIs for classifying MCI-C and MCI-NC were up to 65%, and the region combining hippocampus and parahippocampal gyrus (11,031 voxels) were superior to other regions. From the results, they also suggested that covariance between information encoded in the ROIs may help classification. The regions selected using SVM-RFE were widely distributed across the brain, which is similar to our results on the LPBA40 atlas. This also suggests that inter-regional covariance or correlation may play an important role as a biomarker for early detection of AD.

As Faria et al. (2012) noted, a typical whole brain MR image has approximately more than hundreds of thousands of voxels, and correlations between these enormous number of voxels exceed 5 billion. Moreover, the signal from each voxel is so noisy that it is practically challenging for us to produce a good feature representation for a classification task from the high-dimensional original data. Thus, future work toward challenges of learning automatically hidden topological structures or deep architectures from the original data such as unsupervised feature learning (Coates et al., 2011) and deep learning (Bengio, 2009) could allow us to identify a good representation of features for classification in various neuroimaging data.

5. Conclusions

In conclusion, this study showed that the performance of SVM-based classification of MCI using GM volumes from structural MRI at the baseline differs depending on the choice of atlases that defines ROIs. LPBA40, a population-based probabilistic atlas, was superior to AAL, a single-subject atlas, in classification performance using the SVM-RFE procedure. The result suggests that feature selection is crucial to improve classification performance and that the feature selection method based on the SVM-RFE algorithm effectively enhanced the classification accuracy regardless of the choice of atlas. The choice of atlases for feature extraction is also important when using no feature selection. The appropriate selection of ROIs combined with a feature selection technique in a voxel-based approach has the potential of further improving the classification performance. Moreover, atlas-based parcellation methods can be applied to analyses using other modalities such as resting state functional connectivity MRI studies (Wang et al., 2009; Faria et al., 2012) and multi-modal studies combining structural MRI with other modalities. This study will provide implications for future atlas-based analyses using multivariate pattern analysis methods on a wide range of issues and modalities.

Acknowledgments

Appendix A. Supplementary data

Supplementary data associated with this article can be found, in the online version, at http://dx.doi.org/10.1016/j.jneumeth.2013.10.003.

References

Aguilar C, Westman E, Muehlboeck J-S, Mecocci P, Vellas B, Tsolaki M, et al. Different multivariate techniques for automated classification of MRI data in Alzheimer's disease and mild cognitive impairment. Psychiatry Res 2013;212:89–98.

Albert MS, DeKosky ST, Dickson D, Dubois B, Feldman HH, Fox NC, et al. The diagnosis of mild cognitive impairment due to Alzheimer's disease: recommendations from the National Institute on Aging-Alzheimer's Association workgroups on diagnostic guidelines for Alzheimer's disease. Alzheimers Dement 2011;7:270–9.

Amunts K, Schleicher A, Zilles K. Cytoarchitecture of the cerebral cortex—more than localization. Neuroimage 2007;37:1061–5.

Ashburner J. A fast diffeomorphic image registration algorithm. Neuroimage 2007;38:95–113.

Ashburner J, Friston KJ. Voxel-based morphometry—the methods. Neuroimage 2000;11:805–21.

Ashburner J, Friston KJ. Unified segmentation. Neuroimage 2005;26:839–51.

Bengio Y. Learning deep architectures for AI. Foundat and Trends Mach Learn 2009;2:1–127.

Braak H, Thal DR, Ghebremedhin E, Del Tredici K. Stages of the pathologic process in Alzheimer disease: age categories from 1 to 100 years. J Neuropathol Exp Neurol 2011;70:960–9.

Brodmann K. Vergleichende Lokalisationslehre der Großhirnrinde in ihren Prinzipien dargestellt auf Grund des Zellenbaues. Leipzig: Barth; 1909.

Cabezas M, Oliver A, Lladó X, Freixenet J, Cuadra MB. A review of atlas-based segmentation for magnetic resonance brain images. Comput Methods Programs Biomed 2011;104:e158–77.

Chance SA, Casanova MF, Switala AE, Crow TJ, Esiri MM. Minicolumn thinning in temporal lobe association cortex but not primary auditory cortex in normal human ageing. Acta Neuropathol 2006;111:459–64.

Chance SA, Clover L, Cousijn H, Currah L, Pettingill R, Esiri MM. Microanatomical correlates of cognitive ability and decline: normal ageing, MCI, and Alzheimer's disease. Cereb Cortex 2011;21:1870–8.

Chang C-C, Lin C-J. LIBSVM. A library for support vector machines. ACM Trans Intell Syst Technol 2011;2, 27:1–27.

Cho Y, Seong J-K, Jeong Y, Shin SY. Alzheimer's Disease Neuroimaging Initiative Individual subject classification for Alzheimer's disease based on incremental learning using a spatial frequency representation of cortical thickness data. Neuroimage 2012;59:2217–30.

Chu C, Hsu A-L, Chou K-H, Bandettini P, Lin C. Alzheimer's Disease Neuroimaging Initiative Does feature selection improve classification accuracy? Impact of sample size and feature selection on classification using anatomical magnetic resonance images. Neuroimage 2012;60:59–70.

Coates A, Lee H, Ng AY. An analysis of single-layer networks in unsupervised feature learning. In: Proceedings of the 14th International Conference on Artificial Intelligence and Statistics (AISTATS). JMLR W&CP 15; 2011.

Cui Y, Liu B, Luo S, Zhen X, Fan M, Liu T, et al. Identification of conversion from mild cognitive impairment to Alzheimer's disease using multivariate predictors. PLoS ONE 2011;6:e21896.

Cuingnet R, Gerardin E, Tessieras J, Auzias G, Lehéricy S, Habert M-O, et al. Automatic classification of patients with Alzheimer's disease from structural MRI: a comparison of ten methods using the ADNI database. Neuroimage 2011;56: 766–81.

Davatzikos C, Bhatt P, Shaw LM, Batmanghelich KN, Trojanowski JQ. Prediction of MCI to AD conversion, via MRI, CSF biomarkers, and pattern classification. Neurobiol Aging 2011;32(2322):e19–27.

Desikan RS, Ségonne F, Fischl B, Quinn BT, Dickerson BC, Blacker D, et al. An automated labeling system for subdividing the human cerebral cortex on MRI scans into gyral based regions of interest. Neuroimage 2006;31:968–80.

Destrieux C, Fischl B, Dale A, Halgren E. Automatic parcellation of human cortical gyri and sulci using standard anatomical nomenclature. Neuroimage 2010;53:1–15.

Devanand DP, Van Heertum RL, Kegeles LS, Liu X, Jin ZH, Pradhaban G, et al. (99m)Tc hexamethyl-propylene-aminoxime single-photon emission computed tomography prediction of conversion from mild cognitive impairment to Alzheimer disease. Am J Geriatr Psychiatry 2010;18:959–72.

Devlin JT, Poldrack RA. In praise of tedious anatomy. Neuroimage 2007;37:1033–41.

Eskildsen SF, Coupé P, García-Lorenzo D, Fonov V, Pruessner JC, Collins DL, et al. Prediction of Alzheimer's disease in subjects with mild cognitive impairment from the ADNI cohort using patterns of cortical thinning. Neuroimage 2013;65:511–21.

Evans AC, Janke AL, Collins DL, Baillet S. Brain templates and atlases. Neuroimage 2012;62:911–22.

Fan Y, Shen D, Gur RC, Gur RE, Davatzikos C. COMPARE. Classification of morphological patterns using adaptive regional elements. IEEE Trans Med Imaging 2007;26:93–105.

Faria AV, Joel SE, Zhang Y, Oishi K, van Zjil PCM, Miller MI, et al. Atlas-based analysis of resting-state functional connectivity: evaluation for reproducibility and multimodal anatomy-function correlation studies. Neuroimage 2012;61:613–21.

Ferreira LK, Diniz BS, Forlenza OV, Busatto GF, Zanetti MV. Neurostructural predictors of Alzheimer's disease: a meta-analysis of VBM studies. Neurobiol Aging 2011;32:1733–41.

Folstein MF, Folstein SE, McHugh PR. 'Mini-mental state'. A practical method for grading the cognitive state of patients for the clinician. J Psychiatr Res 1975;12:189–98.

Frisoni GB, Fox NC, Jack CR, Scheltens P, Thompson PM. The clinical use of structural MRI in Alzheimer disease. Nat Rev Neurol 2010;6:67–77.

Guyon I, Weston J, Barnhill S, Vapnik V. Gene selection for cancer classification using support vector machines. Mach Learn 2002;46:389–422.

Habeck C, Foster NL, Perneczky R, Kurz A, Alexopoulos P, Koeppe RA, et al. Multivariate and univariate neuroimaging biomarkers of Alzheimer's disease. Neuroimage 2008;40:1503–15.

Holmes CJ, Hoge R, Collins L, Woods R, Toga AW, Evans AC. Enhancement of MR images using registration for signal averaging. J Comput Assist Tomogr 1998;22:324–33.

Homma A, Fukuzawa K, Tsukada Y, Ishii T, Hasegawa K, Mohs RC. Development of a Japanese version of Alzheimer's Disease Assessment Scale (ADAS). Jpn J Geriatr Psychiatry 1992;3:647–55.

Hsu C-W, Chang C-C, Lin C-J. A practical guide to support vector classification. Tech. rep. Department of Computer Science, National Taiwan University; 2003.

Jack CR, Albert MS, Knopman DS, McKhann GM, Sperling RA, Carrillo MC, et al. Introduction to the recommendations from the National Institute on Aging-Alzheimer's Association workgroups on diagnostic guidelines for Alzheimer's disease. Alzheimers Dement 2011;7:257–62.

Karas GB, Scheltens P, Rombouts SARB, Visser PJ, van Schijndel RA, Fox NC, et al. Global and local gray matter loss in mild cognitive impairment and Alzheimer's disease. Neuroimage 2004;23:708–16.

Kawashima S, Ito K, Kato T. the SEAD-J Study Group Inclusion criteria provide heterogeneity in baseline profiles of patients with mild cognitive impairment: comparison of two prospective cohort studies. BMJ Open 2012;2: e000773.

Kazui H, Watamori TS, Honda R, Mori E. The validation of a Japanese version of the Everyday Memory Checklist. No To Shinkei 2003;55:317–25.

Klöppel S, Abdulkadir A, Jack CR, Koutsouleris N, Mourão-Miranda J, Vemuri P. Diagnostic neuroimaging across diseases. Neuroimage 2012;61:457–63.

Klöppel S, Stonnington CM, Chu C, Draganski B, Scahill RI, Rohrer JD, et al. Automatic classification of MR scans in Alzheimer's disease. Brain 2008;131:681–9.

Knopman DS, DeKosky ST, Cummings JL, Chui H, Corey-Bloom J, Relkin N, et al. Practice parameter: diagnosis of dementia (an evidence-based review) Report of the Quality Standards Subcommittee of the American Academy of Neurology. Neurology 2001;56:1143–53.

Kurth F, Luders E, Gaser C. VBM8-Toolbox manual; 2010 (available at http://dbm.neuro.uni-jena.de/vbm8/VBM8-Manual.pdf).

Mangin J-F, Jouvent E, Cachia A. In-vivo measurement of cortical morphology: means and meanings. Curr Opin Neurol 2010;23:359–67.

McKeith IG, Galasko D, Kosaka K, Perry EK, Dickson DW, Hansen LA, et al. Consensus guidelines for the clinical and pathologic diagnosis of dementia with Lewy bodies (DLB): report of the consortium on DLB international workshop. Neurology 1996;47:1113–24.

McKhann G, Drachman D, Folstein M, Katzman R, Price D, Stadlan EM. Clinical diagnosis of Alzheimer's disease: report of the NINCDS-ADRDA Work Group under the auspices of Department of Health and Human Services Task Force on Alzheimer's Disease. Neurology 1984;34:939–44.

McKhann GM, Albert MS, Grossman M, Miller B, Dickson D, Trojanowski JQ, et al. Clinical and pathological diagnosis of frontotemporal dementia: report of the Work Group on Frontotemporal Dementia and Pick's Disease. Arch Neurol 2001;58:1803–9.

Misra C, Fan Y, Davatzikos C. Baseline and longitudinal patterns of brain atrophy in MCI patients, and their use in prediction of short-term conversion to AD: results from ADNI. Neuroimage 2009;44:1415–22.

Morris JC. The Clinical Dementia Rating (CDR): current version and scoring rules. Neurology 1993;43:2412–4.

Nelson PT, Braak H, Markesbery WR. Neuropathology and cognitive impairment in Alzheimer disease: a complex but coherent relationship. J Neuropathol Exp Neurol 2009;68:1–14.

Nyunt MSZ, Fones C, Niti M, Ng T-P. Criterion-based validity and reliability of the Geriatric Depression Screening Scale (GDS-15) in a large validation sample of community-living Asian older adults. Aging Ment Health 2009;13: 376–82.

Ono M, Kubick S, Abernathey C. Atlas of the cerebral sulci. New York: Thieme; 1990.

Petersen RC, Thomas RG, Grundman M, Bennett D, Doody R, Ferris S, et al. Vitamin E and donepezil for the treatment of mild cognitive impairment. N Engl J Med 2005;352:2379–88.

Rajapakse JC, Giedd JN, Rapoport JL. Statistical approach to segmentation of single-channel cerebral MR images. IEEE Trans Med Imaging 1997;16:176–86.

Robin X, Turck N, Hainard A, Tiberti N, Lisacek F, Sanchez J-C, et al. pROC: an open-source package for R and S+ to analyze and compare ROC curves. BMC Bioinformatics 2011;12:77.

Schmahmann JD, Doyon J, McDonald D, Holmes C, Lavoie K, Hurwitz AS, et al. Three-dimensional MRI atlas of the human cerebellum in proportional stereotaxic space. Neuroimage 1999;10:233–60.

Schmahmann JD, Doyon J, Toga AW, Evans AC, Petrides M. MRI atlas of the human cerebellum. San Diego: Academic Press; 2000.

Shapleske J, Rossell SL, Woodruff PW, David AS. The planum temporale: a systematic, quantitative review of its structural, functional and clinical significance. Brain Res Rev 1999;29:26–49.

Shattuck DW, Mirza M, Adisetiyo V, Hojatkashani C, Salamon G, Narr KL, et al. Construction of a 3D probabilistic atlas of human cortical structures. Neuroimage 2008;39:1064–80.

Stonnington CM, Tan G, Klöppel S, Chu C, Draganski B, Jack CR, et al. Interpreting scan data acquired from multiple scanners: a study with Alzheimer's disease. Neuroimage 2008;39:1180–5.

Sullivan K. Estimates of interrater reliability for the Logical Memory subtest of the Wechsler Memory Scale-Revised. J Clin Exp Neuropsychol 1996;18:707–12.

Tabert MH, Manly JJ, Liu X, Pelton GH, Rosenblum S, Jacobs M, et al. Neuropsychological prediction of conversion to Alzheimer disease in patients with mild cognitive impairment. Arch Gen Psychiatry 2006;63:916–24.

Toga AW, Thompson PM, Mori S, Amunts K, Zilles K. Towards multimodal atlases of the human brain. Nat Rev Neurosci 2006;7:952–66.

Toga AW, Thompson PM. What is where and why it is important. Neuroimage 2007;37:1045–9.

Tohka J, Zijdenbos A, Evans A. Fast and robust parameter estimation for statistical partial volume models in brain MRI. Neuroimage 2004;23:84–97.

Tzourio-Mazoyer N, Hervé PY, Mazoyer B. Neuroanatomy Tool for functional localization, key to brain organization. Neuroimage 2007;37:1059–60.

Tzourio-Mazoyer N, Landeau B, Papathanassiou D, Crivello F, Etard O, Delcroix N, et al. Automated Anatomical Labeling of Activations in SPM Using a Macroscopic Anatomical Parcellation of the MNI MRI Single-Subject Brain. Neuroimage 2002;15:273–89.

Vapnik VN. Statistical learning theory. New York: Wiley; 1998.

Vemuri P, Whitwell JL, Kantarci K, Josephs KA, Parisi JE, Shiung MS, et al. Antemortem MRI based STructural Abnormality iNDex (STAND)-scores correlate with postmortem Braak neurofibrillary tangle stage. Neuroimage 2008;42:559–67.

Wang J, Wang L, Zang Y, Yang H, Tang H, Gong Q, et al. Parcellation-dependent small-world brain functional networks: a resting-state fMRI study. Hum Brain Mapp 2009;30:1511–23.

Whitwell JL, Josephs KA, Murray ME, Kantarci K, Przybelski SA, Weigand SD, et al. MRI correlates of neurofibrillary tangle pathology at autopsy: a voxel-based morphometry study. Neurology 2008;71:743–9.

Whitwell JL, Jack CR, Przybelski SA, Parisi JE, Senjem ML, Boeve BF, et al. Temporoparietal atrophy: a marker of AD pathology independent of clinical diagnosis. Neurobiol Aging 2011;32:1531–41.

Wolz R, Julkunen V, Koikkalainen J, Niskanen E, Zhang DP, Rueckert D, et al. Multimethod analysis of MRI images in early diagnostics of Alzheimer's disease. PLoS ONE 2011;6:e25446.

Yesavage JA, Brink TL, Rose TL, Lum O, Huang V, Adey M, et al. Development and validation of a geriatric depression screening scale: a preliminary report. J Psychiatr Res 1982;17:37–49.

Zheng ZZ. The functional specialization of the planum temporale. J Neurophysiol 2009;102:3079–81.

Zilles K, Amunts K. Centenary of Brodmann's map–conception and fate. Nat Rev Neurosci 2010;11:139–45.

1. 認知症における血管病の重要性

猪原 匡史

要 旨

脳は全身の 2.5％の重量でありながら全血液の 15％が灌流する血流依存度の高い臓器である．そのホメオスターシスを維持するために血液脳関門が準備され，神経機能に必須のイオンやアミノ酸濃度が厳密に管理されている．しかし，厳重な関所が発達した結果，間質液(細胞間隙液)は容易には血管内腔側に戻れず，他の排液路を流れて処理される必要がある．脳にはリンパ'管'が存在せず，血管壁内に間質液の通り道である「血管周囲'リンパ'排液路」が準備され，βアミロイドも一部この排液路を流れる．動脈拍動が本ドレナージの駆動力であり，加齢とともに動脈硬化が進み，駆動力が減少すると，βアミロイドは不溶性凝集物としてこの排液路上あるいは脳内に沈着し，脳アミロイド血管症やアルツハイマー病の増悪因子となる．したがって，動脈硬化をはじめとする「血管病」は血管性認知症のみならず神経変性疾患の病態にも深く関わり，血管病の予防は認知症の先制医療となる．

(脳循環代謝 24：83〜88, 2013)

キーワード：βアミロイド，アミロイド血管症，血管周囲リンパ排液路，認知症，先制医療

1. はじめに

脳は全身の 2.5％の重量でありながら全血液の 15％が灌流する血流依存度の高い臓器である．脳はそのホメオスターシスを維持するために血液脳関門を準備して神経機能に必須のイオンやアミノ酸濃度を厳密に管理している．こうした関所の存在は，ニューロン内外のイオン勾配や神経伝達物質濃度をコントロールするために必須であることから，動物の進化の過程でも淘汰圧として働いたと考えられているが，同時に弊害も生む．このような厳重な関所が発達した結果，間質液(細胞間隙液)は容易には血管内腔側に戻ることができなくなり，他の排液路を流れて処理される必要が生じた．脳以外の臓器ではリンパ管がその役割を担うところであるが，脳にはリンパ'管'が存在しない．

その代替機構として，脳内のリンパ系システムともいえる「血管周囲リンパ排液路」(perivascular lymphatic drainage pathway)が存在する[1]．間質液に含まれるβアミロイド(Aβ)は重合すれば血液脳関門を越えにく

く，この排液路を介して一部処理されている．本稿では，認知症の病態を考えるうえで重要な，血管周囲リンパ排液路に着目する．脳血管は血液の供給系としてのみではなく，老廃物の排泄系という働きも担っており，いわば上下水道という2つの側面を併せ持つ．この脳血管が担う脳循環のダイナミズムを知ることが，血管性認知症のみならずアルツハイマー病など変性型認知症までをも対象とした認知症制圧へのヒントを与えてくれるだろう．

2. βアミロイドの除去機構

若年性アルツハイマー病を除き，高齢者の孤発性アルツハイマー病の主要因は，加齢に伴う Aβ 除去能の低下である[2]．

βアミロイドの除去機構には，以下の3つの代表的機構(3つの D)が知られている．つまり，Delivery, Drainage, Degradation である(図 1)[3]．

1) Transcytotic Delivery —トランスサイトーシスによる血管内腔への排出— lipoprotein receptor related protein-1(LRP-1)[4]や cellular prion protein[5]を介して，毛細血管の反内腔(脳実質)側から内腔側へ Aβ がトランスサイトーシスにより排出輸送される経路

2) Perivascular Drainage —血管周囲リンパ排液路を介

国立循環器病研究センター脳神経内科
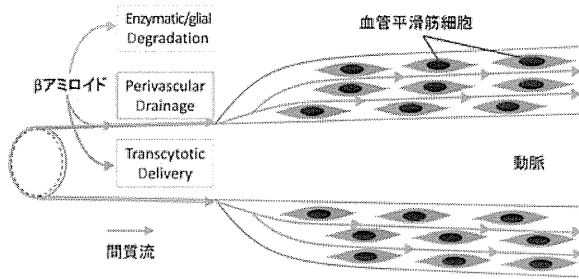〒 565-8565 大阪府吹田市藤白台 5 丁目 7 番 1 号
E-mail: ihara@ncvc.go.jp

図 1. Aβ のクリアランス機構(3 つの D)
βアミロイド(Aβ)のクリアランス(除去)機構には，3 つの代表的機構が知られている．つまり，1. Transcytotic Delivery — 毛細血管の反内腔(脳実質)側から内腔側へのトランスサイトーシスによる輸送，2. Perivascular Drainage — 血管周囲リンパ排液路を流れる間質流(細胞間隙流)にのった輸送，3. Enzymatic/glial Degradation — Aβ を分解する作用のある酵素あるいはグリア(アストロサイトやミクログリア)による分解である．この 3 つの除去機構は互いに相補的に働き，Aβ の蓄積を防いでいるが，加齢や動脈硬化などにより，ひとたびその均衡が破れると，Aβ の脳内蓄積が始まると考えられる．各機構の寄与度については本文を参照されたい．(文献 3 より改変引用)
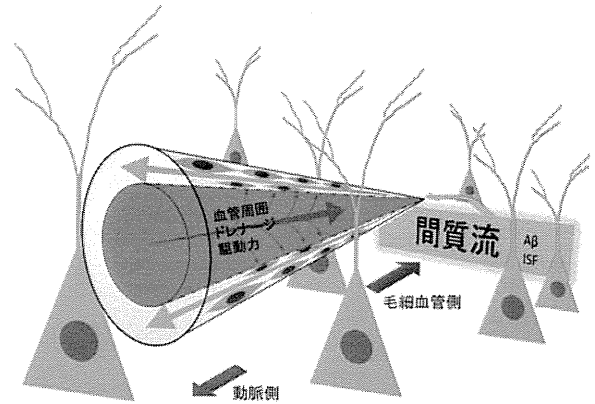

図 2. 血管周囲リンパ排液路の模式図
脳内の毛細血管や動脈壁の基底膜が上述した血管周囲リンパ排液路を構成しており，この経路は Aβ を含む間質液の高速排液システムである．このリンパ排液路は，分子が細胞外腔を拡散する速度よりもずっと早い．動脈拍動がこの血管周囲リンパ排液路の駆動力になっており，本排液路は血流の方向と反対に流れる．脳内に注入された可溶性トレーサーは 10 分以内に軟髄膜血管の基底膜へ到達する．ISF, interstitial fluid．(文献 3 より改変引用)

した排出 — Aβ を含む間質流が血管中膜基底膜層を流れて最終的に髄液や頸部リンパ節に輸送される経路[6]

3) Enzymatic/glial Degradation — Aβ 分解酵素やグリアによる分解 — Neprilysin, insulin-degrading enzyme, plasmin, angiotensin-converting enzyme などのプロテアーゼやグリア(アストロサイトやミクログリア)の働きによる Aβ 分解経路[7]

この 3 つの機構の比率に関して，^{125}I-Aβ40 を用いたマウス脳(尾状核)への注入実験の結果が報告されている．注入後 5 時間までの観察では，血管内腔への排出が 73.8%，血管周囲リンパ排液路を介したと考えられる髄液への移行が 10.7%，脳内での残存が 15.6% であった．したがって，トランスサイトーシスによる血管内腔への排出と血管周囲リンパ排液路を介した排出が Aβ の主たる排出経路と考えられるが，後者への依存度が大きくなる機序として，a. Aβ 濃度の上昇[8,9]；b. アミロイド前駆体遺伝子変異(Dutch/Iowa 変異)[10]；c. Aβ42 増加[10]が知られており，血管周囲リンパ排液路を介した Aβ の排泄機構が，加齢やアルツハイマー病との関連で重要である．

3. 血管壁に沿う Aβ のドレナージ経路 — 血管周囲リンパ排液路

血管周囲リンパ排液路の存在が示唆されたのは 1860 年台に Schwalbe が，大槽に注入された墨汁が 1 分以内に頸部リンパ節に検出されたことに遡る[11]．その後，Bradbury や Cserr らによって，1)髄腔に注入されたトレーサーは篩板を介して頸部リンパ節に流れ込む，2)尾状核に注入されたトレーサーは脳脊髄液とは無関係な経路で頸部リンパ節に流れ込む，3)放射性同位体でラベルされたトレーサーを脳実質内に注入すると頭蓋内では動脈壁に沿って観察される，という事実が明らかにされ，その存在が注目されるようになった[11~13]．さらに，1990 年台初頭に Zhang らが中心となり，1)ラットの線条体に注入された墨汁は拡張した血管周囲腔に近接して存在し，中大脳動脈枝から Willis 動脈輪に沿い，さらには嗅動脈 — 篩骨動脈に沿って篩板に到達する，2)さらに篩板を通り鼻腔リンパ管から頸部リンパ節にまで至る，という報告がなされた[14]．その後の Kida ら[15]や Johnston ら[16]の報告も上記経路の存在を支持するものであった．

その後の Carare らによる詳細な観察の結果，脳内の毛細血管や動脈壁の基底膜が上述した血管周囲リンパ排液路を構成しており，この経路は間質液の高速排液システムであることが示された[17]．このリンパ排液路は，分子が細胞外腔を拡散する速度よりもずっと早く，間質液は，脳内や軟髄膜内の動脈壁に沿ってほぼ即座に排出される(図 2)．可溶性のトレーサーを脳内に注入すると 10 分以内に軟髄膜血管の基底膜へ到達する．なお，この排液路は動脈壁内に存在する経路であって，Virchow-Robin 腔とは異なるものであることには注意を要す．

理論モデルでは，動脈拍動がこのリンパ排液路の駆動力になっており，その力は，心臓由来の脈波に続いて生じる反射波が生み出す遠心力によってもたらされることが証明されている[18]．Aβ は脳底部の中大脳動脈や脳底動脈の壁には検出されるが，頸部内頸動脈には検出されないことから[19]，血管周囲リンパ排液路を流れる溶質は，脳底部で血管壁を離れ，局所のリンパ節に流れ込むと考えられている[6]．頸動脈鞘内には内頸動脈と隣接してリンパ節が平均 12 個存在しており，これらのリンパ節が溶質の回収装置として働いていると考えられる[20]．下丘に注入された Cy5-Aβ40 も 30 分以内には，尾状核や嗅球の血管壁のみならず，頸部リンパ節に検出されることも本経路を考えるうえで興味深い[21]．上述した ^{125}I-Aβ40 を用いた実験では，血中に検出された ^{125}I-Aβ40 をすべてトランスサイトーシスによる血管内腔への排泄とカウントしているが[10]，血管周囲リンパ排液路を介して排泄される Aβ も最終的には血中に回収される（髄液→血中あるいはリンパ節→血中）ことから，血管周囲リンパ排液路を過小評価していた可能性も否定できず，本経路が Aβ クリアランスに果たす役割は実際にはもっと大きいのかもしれない．

4. 血管周囲リンパ排液路が破綻する病態

興味深いことに，このリンパ排液路は，初期の脳アミロイド血管症の Aβ 沈着部位に合致している[6]．すなわち，リンパ排液路の経路である中膜平滑筋基底膜から Aβ の蓄積が始まる．したがって，本経路のうっ滞が脳アミロイド血管症の病態と密接に関連する可能性がある．実際，老齢マウスや脳アミロイド血管症を呈したマウスでは間質流が障害されており[22]，さらに脳アミロイド血管症モデルマウスの両側総頸動脈を人工的に狭窄させると脳アミロイド血管症の病態が加速するなど[23]，加齢・動脈硬化や Aβ 沈着による血管拍動性の低下が脳アミロイド血管症の増悪因子として働く可能性が高い．Neprilysin の濃度が低下したり[24]，LRP1 の発現レベルが低下すると[9]，Aβ のクリアランスが障害され，脳アミロイド血管症を招くことも報告されており，3 つの Aβ 処理系は相補的に機能して Aβ の蓄積を防いでいるのであろう．

クリアランス機構が破綻して血管壁にタンパク質が蓄積するような病態が protein-elimination failure arteriopathies（PEFA）と総称されることがある（図 3）[25]．Aβ 以外でも，gelsolin，cystatin C，transthyretin は家族性脳アミロイド血管症を背景に，脳出血や認知症の原因になり，とくに後二者は脳以外の臓器の血管に
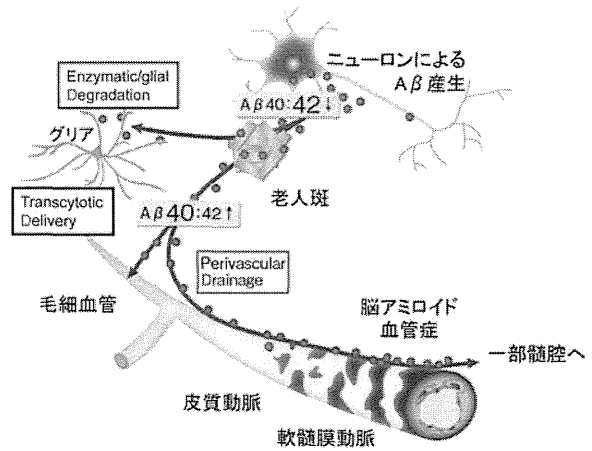

図 3. Protein elimination failure arteriopathy の一型としての脳アミロイド血管症
クリアランス機構が破綻して血管壁にタンパク質が蓄積するような病態が protein-elimination failure arteriopathies（PEFA）と総称され，脳アミロイド血管症をも含む大きな疾患概念である．間質液中の Aβ が髄液へ移行するためには，血管周囲リンパ排液路を流れ，軟膜を透過する必要があり，血管周囲リンパ排液路の駆動力が低下する状況，すなわち，年齢，細動脈硬化，そして脳アミロイド血管症などの存在下では Aβ の髄液移行が減少することになる．とくに易凝集性の Aβ42 は老人斑や毛細血管壁での沈着が主となり，髄腔内まで到達しにくくなると考えられる．（文献 25 より改変引用）

も蓄積する[26]．また，Notch3 遺伝子変異によって起こる遺伝性の血管性認知症である cerebral autosomal dominant arteriopathy with subcortical infarcts and leukoencephalopathy（CADASIL）では，血管平滑筋細胞より産生される Notch3 が血管壁に蓄積し granular osmiophilic material（GOM）の形成に関与するが[27]，これも PEFA の一型であるとも考えられている．GOM は皮膚を含め末梢血管でも観察されることから，このようなドレナージ経路の破綻は脳以外でも起こりうる現象であるともいえる．

5. 脳アミロイド血管症が引き金を引く悪循環

脳アミロイド血管症の存在は，重度になると脳の循環不全を招くため，低酸素誘導因子[28]やエネルギー不全[29]を介して β セクレターゼ 1（BACE1）を誘導し，さらなる Aβ の産生増加を招く（図 4）．したがって脳アミロイド血管症が一旦完成すると，血管周囲リンパ排液路の破綻により Aβ を十分に排出できないにもかかわらず，その産生は亢進し，Aβ 蓄積への悪循環を形成する[30]．

6. アルツハイマー病の免疫療法との関連

　欧米を中心に臨床試験が行われていたアルツハイマー病のAβワクチン療法において，老人斑が消失した部位で，却って脳アミロイド血管症が悪化したという所見が報告された[31]．この現象は，すでにリンパ排液路がうっ滞していた患者で，老人斑から溶出したAβがさらに脳アミロイド血管症を悪化させたからとも解釈されている[32]（図4）．また，Bapineuzumabによる受動免疫療法時にしばしば観察されたamyloid-related imaging abnormalities（ARIA）の病態との関連では，可溶化したAβが血管周囲リンパ排液路に流れ込むも十分ドレナージされずに溢れて浮腫性変化が生じたものがARIA-E（edema）であり，血管壁のAβが中途半端に引き抜かれたことにより血管壁が脆弱化し出血性変化が生じたものがARIA-H（hemorrhage）と考えられており，その程度は免疫療法前の脳アミロイド血管症の程度やAβクリアランス効率により規定される[33]．したがって，アルツハイマー病の免疫療法が将来実現した暁には，少なくとも高度の脳アミロイド血管症の患者はその適応から除外されるべきといえるだろう．さらに，ドレナージを改善させる血管作動性薬剤の併用など，本ドレナージ経路の健全性を高める方策が免疫療法の成否の鍵をも握るかもしれない．

7. おわりに

　加齢や脳アミロイド血管症に伴い，血管拍動性が低下しドレナージ経路が障害されAβの蓄積が加速することから，アルツハイマー病の治療に「血管拍動性をいかに維持するか？」言い換えれば，「いかに血管病を予防するか？」という視点が重要になってくる．かつて脳血管障害とアルツハイマー病を代表とする神経変性疾患は，高齢者で合併することこそあれ，互いに相容れない疾患概念とも考えられていた．しかし，血管拍動性を維持することが脳内リンパ系の通過性を高め，ひいてはAβの沈着をも防ぐ最良の方法となりうることから，生理的にも病理的にも重要なこの血管周囲リンパ排液路のさらなる解明が，アルツハイマー病を含む様々な疾患の病態解明に一筋の光明を与えるだろう．神経変性疾患としてのアルツハイマー病研究は目覚ましい進展を遂げてきた．そこに，血管病の視点からのアルツハイマー病研究が加わることで，アルツハイマー病の根治療法の確立が早晩実現することを願ってやまない．
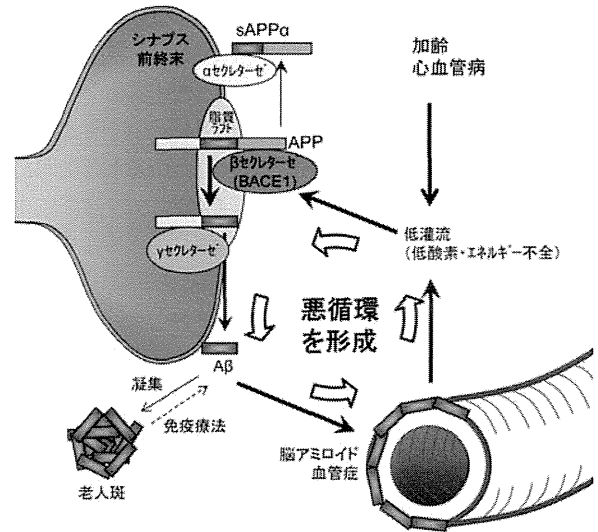

図4. 脳アミロイド血管症が招く悪循環機序
重度の脳アミロイド血管症は，脳の循環不全を招き，低酸素誘導因子やエネルギー不全を介してBACE1を誘導し，さらなるAβの産生増加を招くと考えられる．脳アミロイド血管症により，すでに血管周囲リンパ排液路が閉塞していれば，この悪循環を断ち切ることは甚だ困難であり，免疫療法によって老人斑から可溶化したAβは却って悪循環のサイクルを回転させ，病態を悪化させる可能性すらある．（文献30より改変引用）

文　　献

1) 猪原匡史，Carare RO，Weller RO：脳にもリンパ系があるのですか？ Clin Neurosci 30: 1076, 2012

2) Weller RO, Subash M, Preston SD, Mazanti I, Carare RO: Perivascular drainage of amyloid-beta peptides from the brain and its failure in cerebral amyloid angiopathy and Alzheimer's disease. Brain Pathol 18: 253–266, 2008

3) 猪原匡史，田口明彦：βアミロイドの血管周囲リンパ排液路を介したクリアランス．細胞工学 31: 1113–1118, 2012

4) Davis J, Xu F, Deane R, Romanov G, Previti ML, Zeigler K, Zlokovic BV, Van Nostrand WE: Early-onset and robust cerebral microvascular accumulation of amyloid beta-protein in transgenic mice expressing low levels of a vasculo-tropic Dutch/Iowa mutant form of amyloid beta-protein precursor. J Biol Chem 279: 20296–20306, 2004

5) Pflanzner T, Petsch B, André-Dohmen B, Müller-Schiffmann A, Tschickardt S, Weggen S, Stitz L, Korth C, Pietrzik CU: Cellular prion protein participates in amyloid-β transcytosis across the blood-brain barrier. J Cereb Blood Flow Metab 32: 628–632, 2012

6) Weller RO, Djuanda E, Yow HY, Carare RO: Lymphatic drainage of the brain and the pathophysiology of neurological disease. Acta Neuropathol 117: 1–14, 2009

7) Vardy ER, Catto AJ, Hooper NM: Proteolytic mechanisms

in amyloid-beta metabolism: therapeutic implications for Alzheimer's disease. Trends Mol Med 11: 464–472, 2005

8) Hsiao K, Chapman P, Nilsen S, Eckman C, Harigaya Y, Younkin S, Yang F, Cole G: Correlative memory deficits, Abeta elevation, and amyloid plaques in transgenic mice. Science 274: 99–102, 1996

9) Shibata M, Yamada S, Kumar SR, Calero M, Bading J, Frangione B, Holtzman DM, Miller CA, Strickland DK, Ghiso J, Zlokovic BV: Clearance of Alzheimer's amyloid-ss(1-40) peptide from brain by LDL receptor-related protein-1 at the blood-brain barrier. J Clin Invest 106: 1489–1499, 2000

10) Deane R, Wu Z, Sagare A, Davis J, Du Yan S, Hamm K, Xu F, Parisi M, LaRue B, Hu HW, Spijkers P, Guo H, Song X, Lenting PJ, Van Nostrand WE, Zlokovic BV: LRP/amyloid beta-peptide interaction mediates differential brain efflux of Abeta isoforms. Neuron 43: 333–344, 2004

11) Schwalbe G: Der Arachnoidalraum, ein Lymphraum und sein Zusammenhang mit dem Perichoroidalraum. Zentralb Med Wiss 7: 465–467, 1869

12) Bradbury MW, Cserr HF, Westrop RJ: Drainage of cerebral interstitial fluid into deep cervical lymph of the rabbit. Am J Physiol 240: F329–F336, 1981

13) Bradbury MW, Westrop RJ: Factors influencing exit of substances from cerebrospinal fluid into deep cervical lymph of the rabbit. J Physiol (Lond) 339: 519–534, 1983

14) Zhang ET, Richards HK, Kida S, Weller RO: Directional and compartmentalised drainage of interstitial fluid and cerebrospinal fluid from the rat brain. Acta Neuropathol 83: 233–239, 1992

15) Kida S, Pantazis A, Weller RO: CSF drains directly from the subarachnoid space into nasal lymphatics in the rat. Anatomy, histology and immunological significance. Neuropathol Appl Neurobiol 19: 480–488, 1993

16) Johnston M, Zakharov A, Papaiconomou C, Salmasi G, Armstrong D: Evidence of connections between cerebrospinal fluid and nasal lymphatic vessels in humans, non-human primates and other mammalian species. Cerebrospinal Fluid Res 1: 2, 2004

17) Carare RO, Bernardes-Silva M, Newman TA, Page AM, Nicoll JA, Perry VH, Weller RO: Solutes, but not cells, drain from the brain parenchyma along basement membranes of capillaries and arteries: significance for cerebral amyloid angiopathy and neuroimmunology. Neuropathol Appl Neurobiol 34: 131–144, 2008

18) Schley D, Carare-Nnadi R, Please CP, Perry VH, Weller RO: Mechanisms to explain the reverse perivascular transport of solutes out of the brain. J Theor Biol 238: 962–974, 2006

19) Shinkai Y, Yoshimura M, Ito Y, Odaka A, Suzuki N, Yanagisawa K, Ihara Y: Amyloid beta-proteins 1-40 and 1-42(43) in the soluble fraction of extra- and intracranial

blood vessels. Ann Neurol 38: 421–428, 1995

20) Clapham R, O'Sullivan E, Weller RO, Carare RO: Cervical lymph nodes are found in direct relationship with the internal carotid artery: significance for the lymphatic drainage of the brain. Clin Anat 23: 43–47, 2010

21) Ball KK, Cruz NF, Mrak RE, Dienel GA: Trafficking of glucose, lactate, and amyloid-beta from the inferior colliculus through perivascular routes. J Cereb Blood Flow Metab 30: 162–176, 2010

22) Hawkes CA, Härtig W, Kacza J, Schliebs R, Weller RO, Nicoll JA, Carare RO: Perivascular drainage of solutes is impaired in the ageing mouse brain and in the presence of cerebral amyloid angiopathy. Acta Neuropathol 121: 431–443, 2011

23) Okamoto Y, Yamamoto T, Kalaria RN, Senzaki H, Maki T, Hase Y, Kitamura A, Washida K, Yamada M, Ito H, Tomimoto H, Takahashi R, Ihara M: Cerebral hypoperfusion accelerates cerebral amyloid angiopathy and promotes cortical microinfarcts. Acta Neuropathol 123: 381–394, 2012

24) Miners JS, Van Helmond Z, Chalmers K, Wilcock G, Love S, Kehoe PG: Decreased expression and activity of neprilysin in Alzheimer disease are associated with cerebral amyloid angiopathy. J Neuropathol Exp Neurol 65: 1012–1021, 2006

25) Herzig MC, Van Nostrand WE, Jucker M: Mechanism of cerebral beta-amyloid angiopathy: murine and cellular models. Brain Pathol 16: 40–54, 2006

26) Revesz T, Ghiso J, Lashley T, Plant G, Rostagno A, Frangione B, Holton JL: Cerebral amyloid angiopathies: a pathologic, biochemical, and genetic view. J Neuropathol Exp Neurol 62: 885–898, 2003

27) Ishiko A, Shimizu A, Nagata E, Takahashi K, Tabira T, Suzuki N: Notch3 ectodomain is a major component of granular osmiophilic material (GOM) in CADASIL. Acta Neuropathol 112: 333–339, 2006

28) Sun X, He G, Qing H, Zhou W, Dobie F, Cai F, Staufenbiel M, Huang LE, Song W: Hypoxia facilitates Alzheimer's disease pathogenesis by up-regulating BACE1 gene expression. Proc Natl Acad Sci USA 103: 18727–18732, 2006

29) Velliquette RA, O'Connor T, Vassar R: Energy inhibition elevates beta-secretase levels and activity and is potentially amyloidogenic in APP transgenic mice: possible early events in Alzheimer's disease pathogenesis. J Neurosci 25: 10874–10883, 2005

30) Kalaria RN, Akinyemi R, Ihara M: Does vascular pathology contribute to Alzheimer changes? J Neurol Sci 322: 141–147, 2012

31) Patton RL, Kalback WM, Esh CL, Kokjohn TA, Van Vickle GD, Luehrs DC, Kuo YM, Lopez J, Brune D, Ferrer I, Masliah E, Newel AJ, Beach TG, Castaño EM, Roher AE: Amyloid-beta peptide remnants in AN-1792-

immunized Alzheimer's disease patients: a biochemical analysis. Am J Pathol 169: 1048–1063, 2006

32）Nicoll JA, Yamada M, Frackowiak J, Mazur-Kolecka B, Weller RO: Cerebral amyloid angiopathy plays a direct role in the pathogenesis of Alzheimer's disease. Pro-CAA position statement. Neurobiol Aging 25: 589–597, 2004

33）Sperling R, Salloway S, Brooks DJ, Tampieri D, Barakos J, Fox NC, Raskind M, Sabbagh M, Honig LS, Porsteinsson AP, Lieberburg I, Arrighi HM, Morris KA, Lu Y, Liu E, Gregg KM, Brashear HR, Kinney GG, Black R, Grund-man M: Amyloid-related imaging abnormalities in patients with Alzheimer's disease treated with bapineuzumab: a retrospective analysis. Lancet Neurol 11: 241–249, 2012

Abstract
Impact of cerebrovascular disease in dementia

Masafumi Ihara

Department of Stroke and Cerebrovascular Diseases, National Cerebral and Cardiovascular Center, Osaka, Japan

With the demographic shift in age in advanced countries inexorably set to progress in the 21st century, dementia will become one of the most important health problems worldwide. The discouraging results of the immunotherapy clinical trials for Alzheimer's disease have shifted scientific attention from the mechanism underlying β amyloid (Aβ) synthesis toward clearance, including a perivascular drainage pathway for Aβ. Theoretical models indicate that arterial pulsations may be the motive force for the drainage of interstitial fluid and solutes. As arteries stiffen with age or with other co-morbid factors, the amplitude of pulsations is reduced, perivascular drainage of Aβ becomes less efficient, and insoluble Aβ is deposited in the drainage pathways as cerebral amyloid angiopathy. This notion is supported by the finding that the distribution of Aβ deposits in the basement membranes of cerebral capillaries and arteries corresponds very closely with the perivascular drainage route. Therefore, therapeutic strategies that enhance the patency of this perivascular drainage pathway with vasoactive drugs may facilitate Aβ removal and help prevent cognitive decline in the elderly. Clinical trials based on this emerging paradigm are warranted to determine whether such a hemodynamic strategy is effective to halt cognitive decline as a preemptive medicine.

Key words: β-amyloid, cerebral amyloid angiopathy, perivascular drainage pathway, dementia, preemptive medicine